

Large-Area All-Textile Pressure Sensors for Monitoring Human Motion and Physiological Signals

Mengmeng Liu, Xiong Pu,* Chunyan Jiang, Ting Liu, Xin Huang, Libo Chen, Chunhua Du, Jiangman Sun, Weiguo Hu,* and Zhong Lin Wang*

Wearable pressure sensors, which can perceive and respond to environmental stimuli, are essential components of smart textiles. Here, large-area all-textile-based pressure-sensor arrays are successfully realized on common fabric substrates. The textile sensor unit achieves high sensitivity (14.4 kPa^{-1}), low detection limit (2 Pa), fast response ($\approx 24 \text{ ms}$), low power consumption ($< 6 \mu\text{W}$), and mechanical stability under harsh deformations. Thanks to these merits, the textile sensor is demonstrated to be able to recognize finger movement, hand gestures, acoustic vibrations, and real-time pulse wave. Furthermore, large-area sensor arrays are successfully fabricated on one textile substrate to spatially map tactile stimuli and can be directly incorporated into a fabric garment for stylish designs without sacrifice of comfort, suggesting great potential in smart textiles or wearable electronics.

Forthcoming smart textiles (also known as E-textiles), where various electronic components such as mechanically sensitive sensors,^[1] electronic skin,^[2] flexible transistors,^[3] energy-harvesting and storage devices,^[4] stretchable electronics^[5] are integrated in yarns, fabrics, or garments, have attracted considerable interest. Wearable pressure or strain sensors, which can “feel” and respond to environmental stimuli, are essential components of E-textiles. Their preliminary applications have been explored for biomonitoring of physiological signals, textile keyboards, and touch-pads, etc. For E-textiles, pressure sensors are required to be highly sensitive (especially in the low-pressure range), flexible, comfortable, lightweight, breathable, or washable. The majority of state-of-art pressure-sensing devices are rigid silicon-based strain sensors fabricated by the micro-electromechanical systems techniques, which can hardly meet these requirements due to their stiffness, low sensitivity, and

limited sensing range.^[2a] Therefore, textile-based flexible pressure sensors, which can be readily incorporated into a garment without much sacrifice of its softness, design versatility, or convenience, are ideal for E-textiles.

Recently, intensive endeavors have been devoted to developing flexible pressure-sensitive devices. A number of “skin-like” sensors^[6] (e.g., electronic skins) have been realized by utilizing capacitive,^[7] piezoelectric,^[8] resistive,^[9] or triboelectric^[10] effects. These pressure sensors based on ultrathin inorganic silicon,^[11] pressure-sensitive rubber,^[12] organic semiconductors,^[13] conducting polymers,^[7a] ionic gels,^[14] or self-powered systems^[15]


have been reported with high sensitivity and excellent flexibility. However, either the fabrication process of these devices could be laborious, or their flat plastic or polymer substrates, such as poly(ethylene terephthalate) (PET), polyimide (PI), poly(dimethylsiloxane) (PDMS), rubber, and paper,^[16] are still inappropriate for smart textiles.

Textiles are ideal vehicles for the design of flexible pressure sensors, especially for wearable electronics with detection purposes of healthcare and human activities, since textile are hygroscopic, soft, breathable, and comfortable to human skin.^[17] Considering the wavy surface of the textile, above-mentioned materials choices and processing techniques are typically unapplicable. Recently, resistive textile-based pressure sensors have been reported with the aid of various nanomaterials, such as fiber-shaped carbon nanotubes (CNT),^[2b,18] graphene,^[19] graphene/polymer nanocomposites,^[20] carbonized silk fabrics,^[21] electrospun nanofibers,^[6a,22] and common cloth coated with carbonaceous materials.^[7b,16b,23] Despite this progress, a whole-textile-based pressure sensor is still required. In addition, large-area textile-based pressure-sensor arrays able to map pressure distributions are seldom reported by far.

Here, we demonstrate a facile and novel approach for fabricating all-textile-based pressure sensors and large-area sensor arrays. The resistive textile sensor unit is composed of a bottom interdigitated textile electrode and a top bridge of CNT-coated cotton fabric. The interdigitated conductive electrodes on common textile (polyester, nylon, etc.) were fabricated by laser-scribing masking and electroless deposition of conformal Ni coatings. The resulting sensor on textile substrate exhibited high sensitivity (14.4 kPa^{-1} for pressure below 3.5 kPa, 7.8 kPa^{-1} for pressure range of 3.5–15 kPa), stable cycling performances

M. Liu, Dr. X. Pu, C. Jiang, T. Liu, X. Huang, L. Chen, Dr. C. Du, Dr. J. Sun, Prof. W. Hu, Prof. Z. L. Wang
Beijing Institute of Nanoenergy and Nanosystems
Chinese Academy of Sciences
National Center for Nanoscience and Technology (NCNST)
Beijing 100083, China
E-mail: puxiong@binn.cas.cn; huweiguo@binn.cas.cn; zlwang@gatech.edu

Prof. Z. L. Wang
School of Materials Science and Engineering
Georgia Institute of Technology
Atlanta, GA 30332-0245, USA

 The ORCID identification number(s) for the author(s) of this article can be found under <https://doi.org/10.1002/adma.201703700>.

DOI: 10.1002/adma.201703700

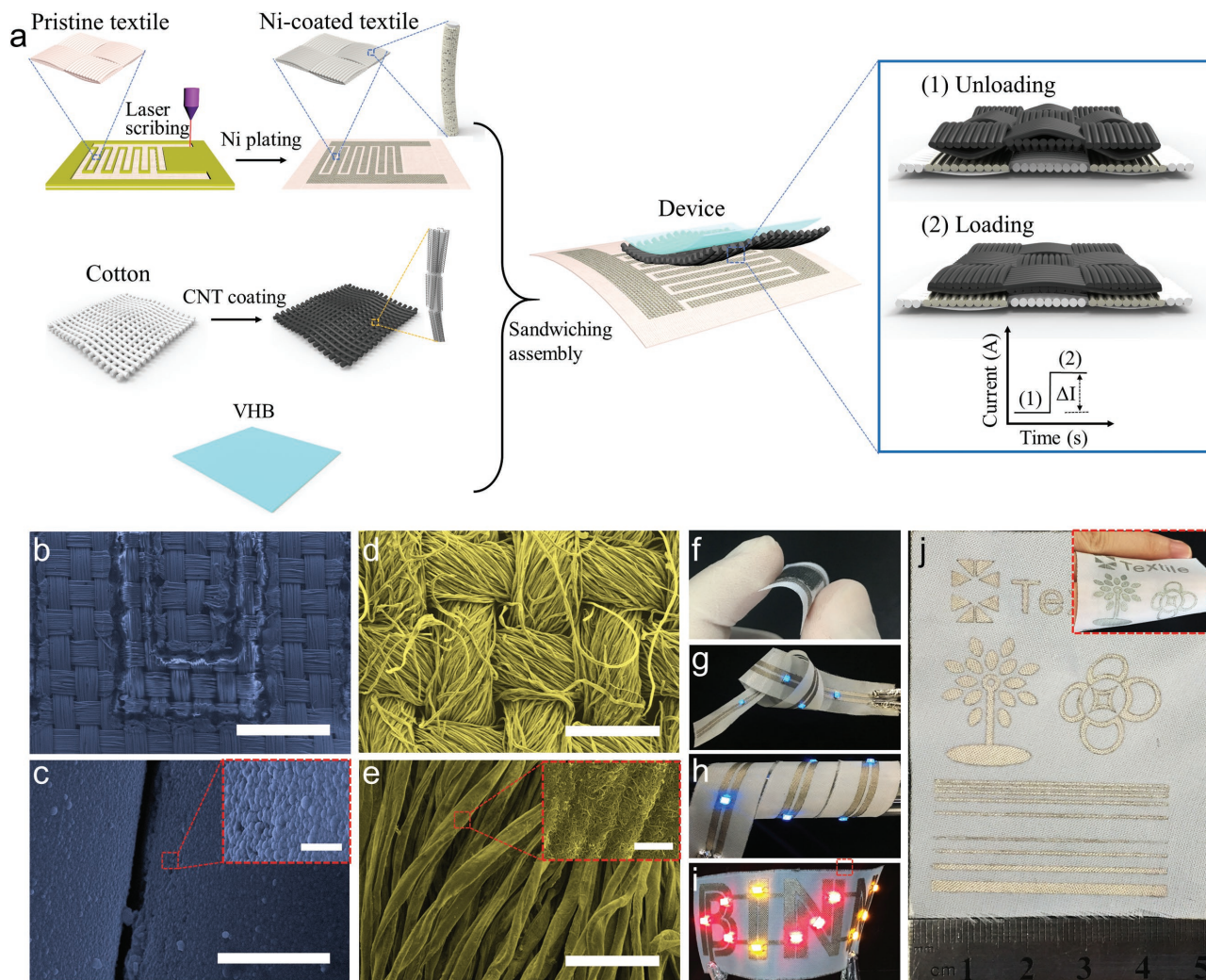


Figure 1. The fabrication of textile-based pressure sensors. a) Schematic illustration of the fabrication procedure of textile pressure sensors. b, c) SEM images of a Ni-coated finger electrode on the textile. d, e) Scanning electron microscopy (SEM) images of the morphology of CNT coating on the cotton fabric at different magnification. f) A photograph showing the bendability of the textile sensor. j) Different conductive drawings fabricated on polyester fabrics. g–i) LEDs lit by a DC source through knotted (g), rolled (h), and bent (i) textile conductive circuits. The scale bars are 1 mm for (b), 3 μm for (c), and 500 μm for (d), 100 μm for (e), and 1 μm for the inset in (e).

(1000 cycles) and a fast response time (≈ 24 ms) and low detection limit (2 Pa). Meanwhile, the fabricated textile pressure sensor could be attached on human skin to detect various forces and vibrations, and monitor real-time pulse wave with low power consumption ($< 6 \mu\text{W}$). In addition, tactile sensor arrays were successfully fabricated and directly incorporated into a fabric garment for pressure mapping.

The pressure-sensing device for wearable E-textiles should be versatile for fashionable and comfortable designs. **Figure 1a** illustrates the fabrication procedure of the all textile-based pressure sensor. As shown schematically in Figure 1a, commercial polyester textile sealed with Kapton tapes on both sides undergoes laser scribing to form mask with desired patterns. The intensity of the laser is controlled to cut through the top Kapton layer but not damage the textile underneath. The polyester textile with Kapton mask then undergoes the electroless deposition (ELD) of conformal Ni coating with a method as we previ-

ously reported.^[4a] After removing the Kapton mask, two Ni electrodes with interdigitated configuration are coated on the textile substrate. Then, a piece of cotton textile dip-coated with CNTs is placed on top of the Ni-coated interdigitated electrodes, followed by covering a thin 3M VHB 9469 (typically acrylate polymers) film for encapsulation. With the mask-aided ELD coating method, a clear gap between two adjacent Ni finger electrodes can be observed and the woven feature of the pristine fabric is maintained (see Figure 1b). At higher magnification, Ni nanoparticles wrapping up the polyester fiber can be observed (see the inset in Figure 1c). Figure 1d, e is the SEM images of the CNTs-coated cotton fabric, showing that the CNT coating is uniform and each individual cotton fiber is decorated with a layer of percolated CNT networks (see the inset in Figure 1e; and Figure S1, Supporting Information). As both the Ni and CNT coatings are thin, the final pressure sensor maintains the mechanical flexibility of pristine textiles, as confirmed by a bent

textile sensor in Figure 1f. For the bottom interdigitated electrodes, finger electrodes width is 0.8 mm and insulating gaps width is 0.4 mm (see Figure S2 in the Supporting Information for the size of the interdigitated textile).

The hierarchical, porous nanostructure of both CNT fabric and nanoparticle-coated Ni textiles provides large surface area, sufficient roughness and elasticity to “feel” the variation of contact resistance when pressure is loaded. Applying an external pressure would cause a small deformation of the porous structures and hence an increase in the contact area between the top CNT fabric bridge and the bottom Ni textile electrodes. Such an increase in the contact area will lead to more conductive pathways between CNTs and Ni film, so the current will increase when increasing the applied pressure, as schematically shown in Figure 1a. A constant voltage of 0.2 V is applied to the bottom Ni interdigitated fabric such that current will flow through each contact tips between the CNTs and Ni coatings, with each tip equivalent to a resistor in the parallel circuit (see Figure S3, Supporting Information). The variation in the contact resistance is majorly responsible for the textile sensor's response to the applied external pressure.^[16b]

This mask-assisted ELD method is able to coat the wavy fabric with various conductive patterns, and could be promising for applications in textile circuits. For demonstration, a series of conductive drawings were fabricated on a polyester fabric (a flower, a tree, an English word of “textile,” triangle arrays, rectangle lines), as shown in Figure 1j. Due to the high conductivity of metal film, the sheet resistance of the Ni textile was measured to be only about 0.7 Ohm sq⁻¹. The Ni-conductive electrode can be bent at curvature radius of 20 mm for 2000 cycles by a linear motor to

confirm the mechanical flexibility and durability. The conductivity of the conductive fabrics shows no obvious degradation (see Figure S4, Supporting Information). Microelectronic devices, such as light-emitting diodes (LEDs) were successfully fabricated on the porous textile surfaces. Figure 1g–i shows that commercial LED cells adhered onto various Ni-coated conductive textiles (see the connecting details between the LED and conductive textile in Figure S5, Supporting Information) can be lighted by a DC current source even at knotted (Figure 1g) or rolled (Figure 1h) conditions. In addition, we designed another pattern on a polyester fabric in the form of four letters, i.e., “BINN,” as shown in Figure 1e. Each letter is composed of two parallel lines of Ni with LED cells attached. The images of shining LEDs with different colors under bending indicate that all connections were stable. This mask-assisted deposition route is also applicable to several different textile substrates. Various patterns with clear interstitials were successfully fabricated on nylon fabrics as well (see Figure S6a, Supporting Information). Figure S6b–h shows line-and-space patterns on the rugged textile substrate. Our method makes it possible to fabricate lines with a minimum gap size of 300 μm, and a minimum linewidth of 300 μm (see Figure S6, Supporting Information). These dimensions are sufficiently small for the attachment of commercial electronic components.^[24]

To explore the pressure responses of the presented sensor, we measured the current responses to different pressures applied on the device. The *I*–*V* curves at different pressures indicate that the response of our device to static pressure is steady and the resistance (slope of *I*–*V* curves) under each applied pressure is constant (see Figure 2a). The sensitivity of the pressure sensor is defined as $S = \delta(\Delta I/I_0)/\delta P$, where ΔI is the relative

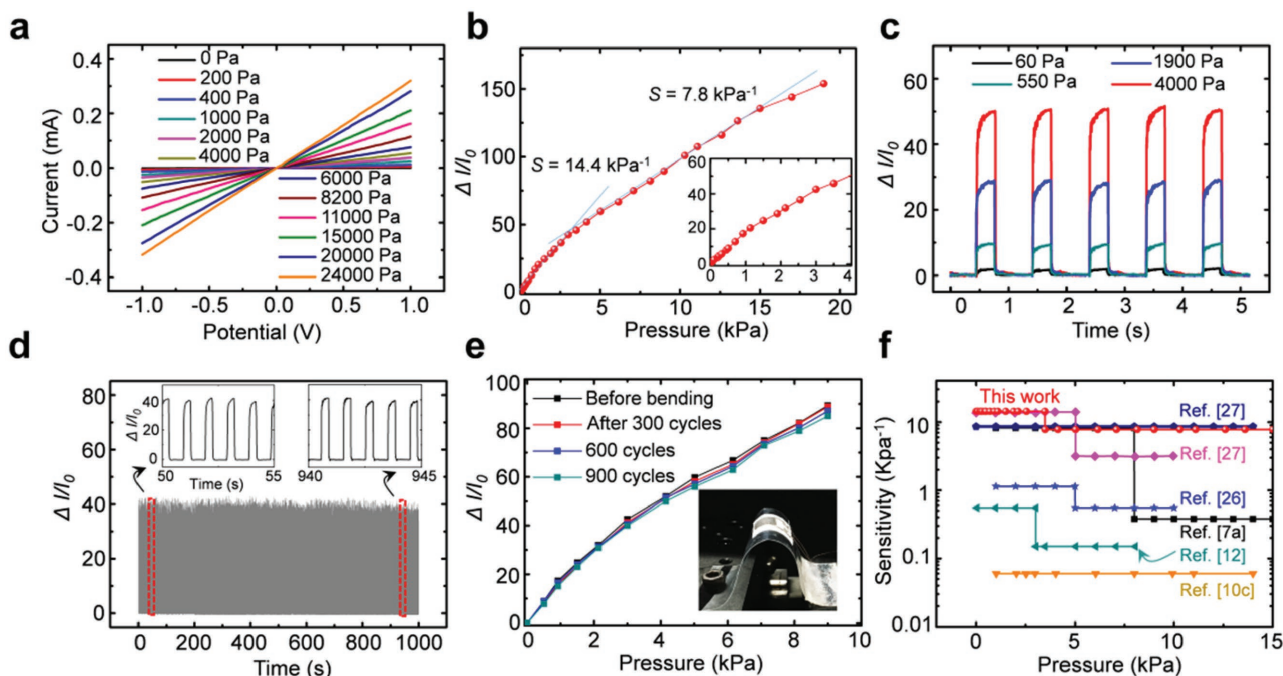


Figure 2. Evaluation of electromechanical performances. a) *I*–*V* curves of the sensor with applied various pressures. b) Recorded current variation ($\Delta I/I_0$)–pressure relationship of three pressure sensors with different amount of CNT coatings. c) Plot of current profiles as a function of time at different pressures applied on the device. d) The durability test under a pressure of 2800 Pa. e) Sensor performance before and after 900 cycles of bending. The inset is a photograph of the bent sensor. f) Sensitivity of our textile-based sensor in comparison with previously reported pressure sensors made of hierarchical graphene on PET,^[27] polymer transistors on PI,^[7a] AuNWs paper on PDMS,^[26] pyramid structure on PET,^[12] and TESMs on PET.^[10c]

change in current, I_0 is current without applied pressure, and P is the applied pressure. The sensitivities were obtained for the textile sensor with cotton fabrics with 15 cycles of CNTs coatings, i.e., 14.4 kPa^{-1} for pressure below 3.5 kPa and 7.8 kPa^{-1} for $3.5\text{--}15 \text{ kPa}$ (see Figure 2b).

Figure 2c shows representative current profiles ($\Delta I/I_0$) of the textile sensor at four different pressures. After ≈ 1000 cycles of repeated loading–unloading under a pressure of 2.9 kPa , the current profiles show no obvious degradation (see Figure 2d), confirming that the performance of the textile sensor is stable for long-term service. In addition, the current responses and the input pressure waves matched well under a pressure of 1.6 kPa (see Figure S7, Supporting Information). The textile sensor is also highly flexible since all the components are based on soft textiles. Furthermore, after repeated bending for over 900 cycles at 25 mm of curvature radius by a linear motor, the performance of the device shows negligible variation (Figure 2e), further confirming its mechanical stability and durability. The inset optical image in Figure 2e shows the bent textile pressure sensor fixed on a linear motor.

Textiles can be intrinsically stretched on account of the fact that woven (wavy) structure can be extended in different directions.^[25] Uniaxial tensile tests were performed to evaluate the mechanical properties of the pristine textile, Ni-coated textile, and the textile sensor (Figure S8, Supporting Information). Optical images of the device at initial state (0% strain) and stretched state (strain $\varepsilon = 3.7\%$) were showed in Figure S8a (Supporting Information). The sensor and Ni-coated textile showed an ultimate failure strain $\varepsilon = 5.2\%$ at a stress of 51.6 and 46.2 MPa , respectively (Figure S8b, Supporting Information). The tests also showed that the device and Ni-coated textile were about 144% and 129% stronger than pristine textile. In addition to the bending tolerance, the textile sensors can tolerate certain degree of linear strain (Figure S9, Supporting Information). After 5 cycles of repeated cyclic stretching to strain $\varepsilon = 3.7\%$, the device shows stable mechanical performance (Figure S9a, Supporting Information). Meanwhile, after the cyclic loading, the sensitivity of the device shows negligible variation (Figure S9b, Supporting Information).

Figure 2f compares the sensitivity obtained in this work with that of pressure sensors reported in the literature. The sensitivity of our approach is generally higher than or comparable with that of pressure sensors with structure of dip-coating Au-nanowire tissue paper,^[26] interlocking nanofibers on PDMS substrate ($1.14\text{--}11.45 \text{ kPa}^{-1}$),^[22] polymer transistors on PI (8.4 kPa^{-1}),^[7a] triboelectric sensor matrices (TESMs) on PET,^[10b] pyramid microstructured PDMS film on PET^[12] and hierarchical graphene (HIE and HIE-LM) on PET (14 kPa^{-1})^[27] and those reported in most of previous literatures^[28] (see Table S1, Supporting Information). We attribute the high sensitivity of our device to the abundant contact interface area of the top CNT fabric with hierarchical nanostructures and bottom textile interdigitated electrodes with Ni nanoparticle coatings.^[9a,24b] Most bottom electrode of resistive skin sensors are based on photolithographic metal, indium tin oxide (ITO), graphene, CNT, or conductive-polymer electrode on flat substrates. Compared to flat substrates, the wavy textile woven from numerous microfibers can supply more contact area between the top and bottom electrodes, and therefore achieved high sensitivity.

Due to the high sensitivity and flexibility of the textile pressure sensor, it was employed to detect finger gestures, hand gestures, and acoustic vibrations. A textile pressure sensor is attached to the curvy skin of an index finger. Once the finger is bent, the contact area between the bottom Ni electrodes and top CNT-coated cotton fabric will increase, leading to the raise in the current correspondingly (see Figure 3a). The current can further increase with the enlargement of bending angles. In addition to bending forces, our pressure sensor can also be used to detect the pressing (Figure 3b), twisting (Figure 3c), and stretching (Figure S10b, Supporting Information) forces. In general, hysteresis of the electrical signal during loading/unloading is one of the critical issues for physical sensors. Sensing performance based on conductive rubber are easily limited by hysteresis effect.^[7a,28a] By switching the state of loading and unloading, few hundred milliseconds are needed to recover the device from stretching/bending state to initial state (Figure S10, Supporting Information).

Thanks to the high sensitivity, our pressure sensor could be also applied to detect acoustic vibrations. To demonstrate such a capability, we attached our sensor to a thin film and positioned them close to a speaker (see Figure 3d). Interestingly, with the speaker turned on, the tiny vibrational forces from music could be accurately recorded. As the speaker turned off, the responding current gradually returned to the initial state (see Figure 3e). In addition, the sensor can be attached to a guitar for tiny vibration recognition (see Figure S11, Supporting Information). Figure 3f shows that a textile sensor was attached onto skin of the neck to noninvasively monitor pressure difference of the muscle movement during speech. As shown in Figure 3g, the device exhibited high sensitivity and distinct current curves when the speaker said different words and phrases such as “Textile,” “Pressure sensor,” and “Go,” respectively. Interestingly, the current decreased during the detection of vibration, vocal signals, and signals from speaker and musical instruments; while the output current signals increased from pressing, bending, twisting of the sensors, which is in accordance with the previous studies.^[19b,29] In general, compared with the loading forces of pressing/bending/twisting, the acoustic and vocal signals always accompany with high-frequency vibrating, which make a tendency to separate the top and bottom textile electrode with each other, as the soft textile substrates cannot deform at high frequency accordingly. The current signals decrease with less contact area between the two electrodes. As for dynamic mechanical force of pressing/bending/twisting at low frequency, the two textile electrodes can respond and recover in time, leading to the current increase.

Figure 3h shows the image of a model hand with pressure sensors on four fingertips connected with textile conductive interconnects. Using mask-assisted deposition method, interdigitated electrodes pattern on fingertip and interconnects pattern on palm were successfully fabricated on a single textile substrate. Integration of four pressure sensors creates a wearable sensor platform to detect the motion of the hand, as shown in Figure 3i. Our device could detect and distinguish the motion of each finger (the index, middle, ring, and little finger) individually and precisely, and the output of each gestures (holding all fingers straight, stretching the index finger and middle finger into a V sign, shaking hands, and holding

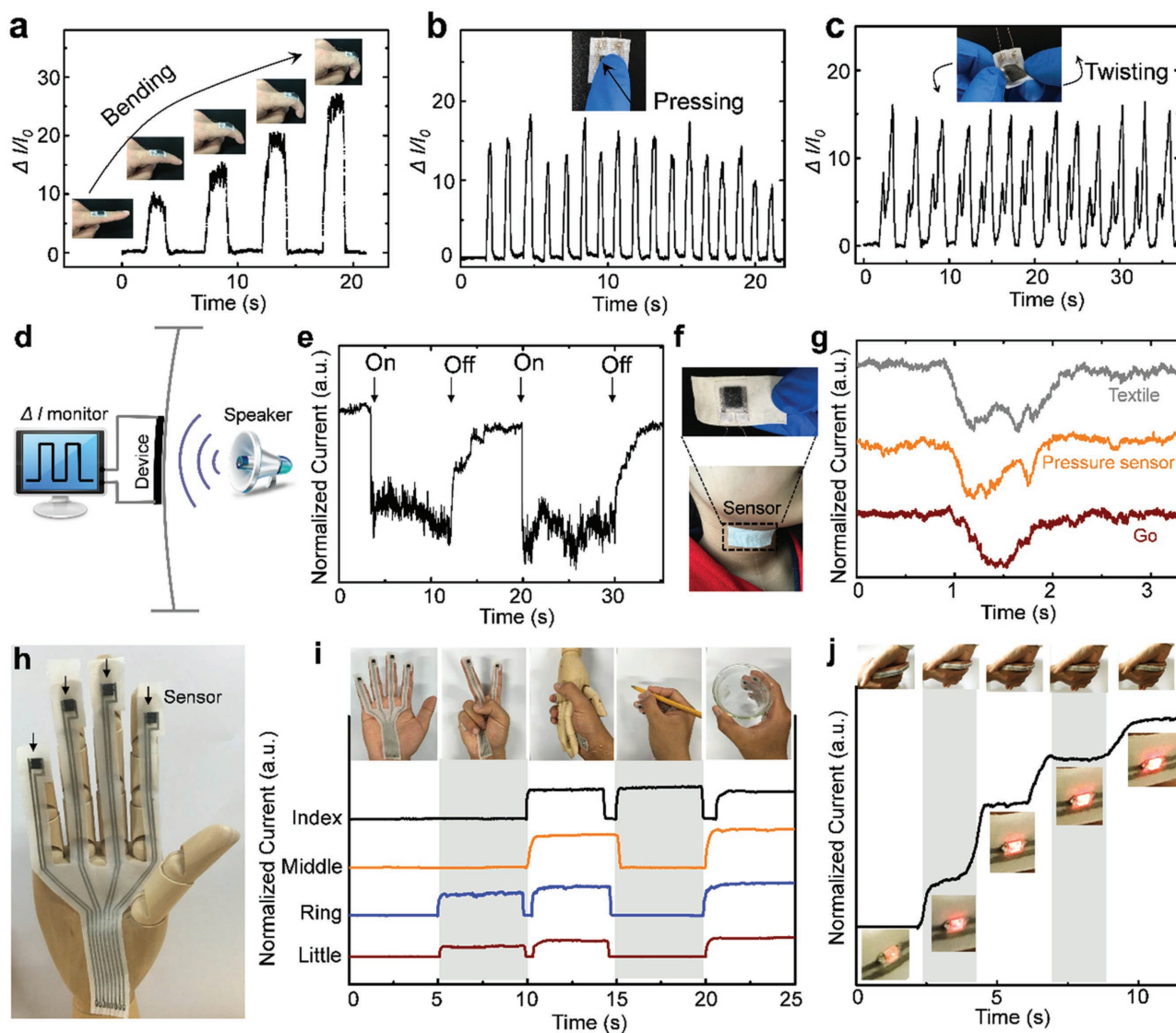


Figure 3. Real-time detection of different mechanical forces and sounds using the textile sensor. a) Optical images and corresponding current signal of a wearable sensor conformally attached to the skin of a bent finger. b,c) Photograph images and current signal responding to dynamic mechanical forces: b) pressing, c) twisting. d,e) Schematic illustration and real-time current signal responding to acoustic vibrations from a piece of music. f,g) Photograph images of device attached to body neck and real-time current signal responding to different words. h) Photograph of an artificial hand covered by textile pressure sensors on different fingers. i) Real-time current signal in response to various hand motions. j) Current signal in response to hand shaking with different pressures. The inset pictures show that a LED cell is turned on when the hands are touched, and the luminescence intensity indicates the pressure of hand shaking. The operating voltage is 3 V.

a pencil or beaker) could be measured to assess the hand gestures. As for pressure sensors, previous works have focused on the optimization of device interfaced with an electronic readout, whereas user interfaces based on a human-readable output have seldom been explored.^[30] A user-interactive pressure-sensor device which provides a real-time visual response through a LED cell adhered to the textile electrode is shown in Figure S12 (Supporting Information). The device was attached on the index finger with pressure sensing area on the fingertip. Figure 3j depicted current response to hand shaking with different pressures. The red LED cell is turned on instantaneous when the two hands touched, and the intensity of the luminescence faithfully indicates the magnitude of the applied pressure

of hand shaking. These demonstrations suggest that our device is flexible, wearable, highly sensitive in the low-pressure range, and facile for integration of more sensing components in a comfortable smart textile.^[24]

Our all-textile pressure sensor is wearable and could be applied for healthcare monitor. One sensor was attached to the artery of a wrist for real-time monitoring the physical force of the pulse beat (see Figure 4a). The fast response time (18–24 ms) and high sensitivity of the pressure sensor provide high resolution to obtain the detailed pulse wave. Figure 4b shows a record of radial artery pressure wave consist of three component waves: percussion wave, tidal wave, and diastolic wave.^[31] Such data can be used to derive the radial

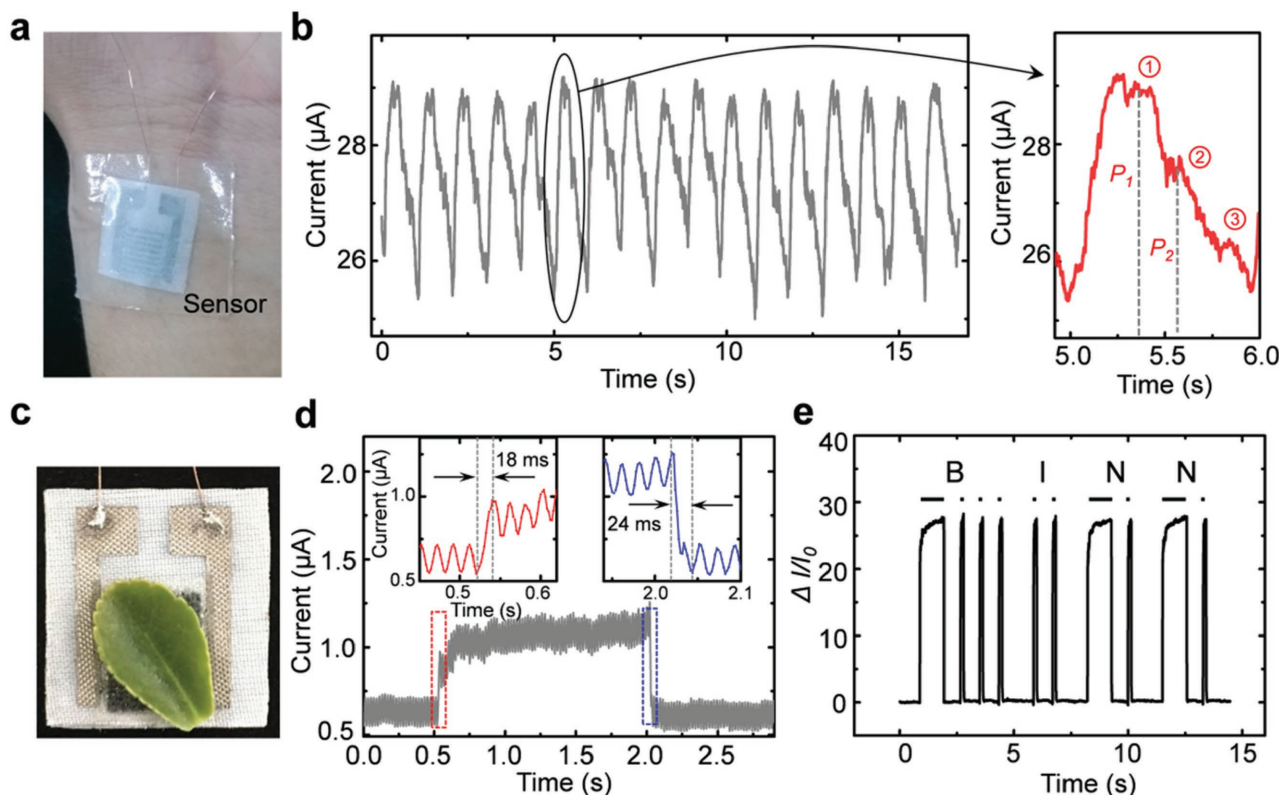


Figure 4. Real-time pulse wave and small strain sensing performance. a) Photograph of a textile pressure sensor attached on the wrist for detection of wrist pulses. b) Original signals of the physical force of radial artery. c,d) Optical image and current curve of our textile sensor pressed by a small leaf. e) Morse code for four letters, i.e., “BINN” produced by touching the sensors.

augmentation index (AI_T), defined as P_2/P_1 in Figure 4b, which is related to arterial stiffness (useful information for diagnosing vascular aging).^[7a]

The detection pressure limit and response/relaxation time of the pressure sensor were also analyzed in Figure 4c,d. The pressure sensor immediately responded to a little leaf pressure of 2 Pa, with response time of 18 ms and a delay of 24 ms under a supplied voltage of 0.2 V. Higher pressure of 2.9 kPa is responded by the pressure sensor immediately with response time of 24 ms and a delay of 30 ms (see Figure S13, Supporting Information). The low detection limit, short response time, and small energy consumption are remarkable better or comparable with several representative previous studies, including those using Au-nanowire-coated tissue paper (13 Pa, 17 ms, and 1.5 V), and micropyramidal conductive composite array (23 Pa, 200 ms, and 0.2 V)^[9a,26] (see Table S1, Supporting Information). In addition, we inputted Morse code by touching the surface of the sensor device, and the curves of the current responses correspond to four characters, i.e., “BINN” (see Figure 4e).

To test the feasibility of tactile sensing for smart textiles, it is desirable to build our sensors into a textile sensing array to spatially map resolved pressure information. **Figure 5a** schematically describes the 4×4 pixels sensing arrays (each is $4.5 \times 4.5 \text{ mm}^2$) on rugged textile substrate. The mask-aided deposition method was used to pattern bottom electrodes with interdigitated geometry and interconnecting Ni wires (see details in Figure S14, Supporting Information). Next, we

sandwiched CNT-coated fabric as top electrode and VHB thin film as encapsulation. This sensing array is flexible can be easily sewed onto a cloth, and can be bent or twisted (see Figure 5b). Figure 5c shows that the sensing array can be conformally attached onto human wrist, and the contact points touched by two fingers were identified (see Figure 5d). When a Z-shaped acrylic plate was placed on the sensor arrays (Figure 5e), the output current intensity can literally represent the touching area, as shown in Figure 5f. Moreover, motion trajectory can be monitored using the pressure-sensing array. When an index finger moves along the surface of sensing array (Figure 5g–i), the motion paths could be clearly tracked (Figure 5j–l).

In summary, we have reported a versatile and facile approach to highly sensitive and flexible textile pressure sensors and sensing arrays. By the combination of mask-assisted Ni-coating and CNT fabric, our method allows for the fabrication of pressure sensors and multipixel arrays directly on cloth without the use of conventional wafer-based technologies. The resulting all-textile pressure sensors achieve high sensitivity (14.4 kPa^{-1}), stable cycling performances (1000 cycles), a fast response time ($\approx 24 \text{ ms}$), low power consumption ($< 6 \text{ μW}$), and mechanical stability under harsh deformations. The devices can act as part of human skin or clothing to detect various external pressures, human activities, and even real-time monitoring of pulse wave. These remarkable features endow our device capabilities of facile integration with other functional devices (e.g., LED cells) for human-readable user-interactive interfaces. Based on the

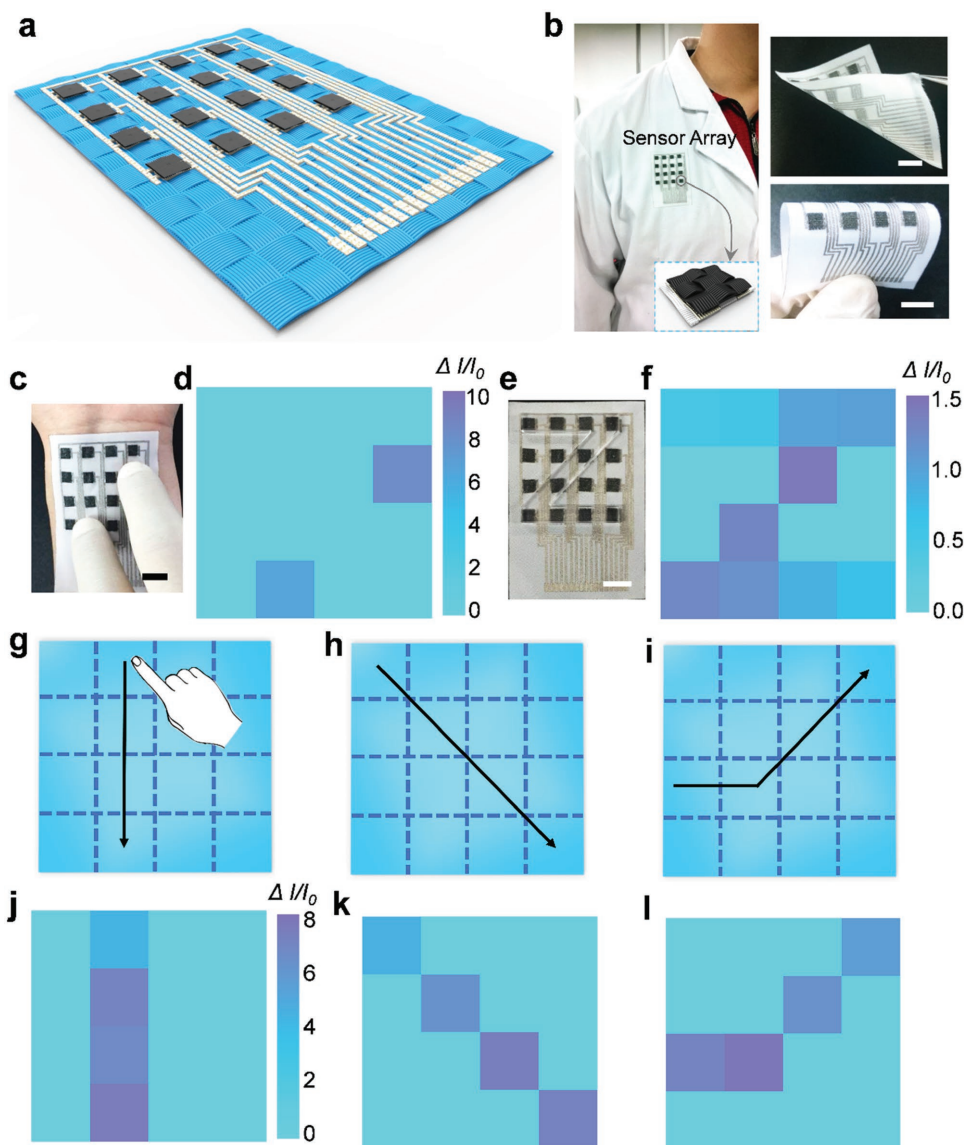


Figure 5. Pressure mapping and trajectory monitoring by the textile-based pressure sensing array. a) Schematic description of a sensor array with 4×4 pixels. b) Photographs of the sensor array sewed on a garment, under bending and twisting. c) A photograph of the sensor array attached on the wrist with touched by two fingers and d) corresponding mapping of the pressure distribution. e,f) A photograph of the sensing array pressed with a Z-shaped acrylic plate (e) and the corresponding current signals of the 16 pixels (f). g–l) Schematic illustrations of the movement of index finger moved over the device (g–i) and corresponding pressure mapping (j–l). The scale bars are 1 cm for (b), (c), and (e).

low-cost fabrication, high performance, flexibility, and human-friendly characteristics, we have presented a route to pressure sensors with great promise in smart textiles or wearable electronics.

Experimental Section

Fabrication of Flexible Pattern and Circuit on Textile: Polyester/nylon textile was first thoroughly cleaned by abundant acetone, alcohol, and deionized (DI) water with a bath sonicator, respectively. Subsequently, both sides of the textile were covered with commercial Kapton tape tightly. A computer-controlled commercial CO₂ laser cutter system was then used to scribe the Kapton into predesigned patterns without damaging the sandwiched textile. Ni was then deposited on the textile

substrate with the aid of the mask via electroless plating similar to the previous report.^[32]

Fabrication of CNT-Coated Fabric and Sensor Fabrication: The CNT ink was prepared by dispersing 1.6 mg mL⁻¹ single-walled carbon nanotubes (SWNTs) in water with 10 mg mL⁻¹ sodium dodecylbenzene sulfonate as surfactant by 1 h sonication.^[33] Then a cotton textile was dipped into the black SWNT ink and dried for 15 cycles, leading to a piece of uniform black fabric with a sheet resistance of 75.4 kΩ sq⁻¹. The sample was then washed with deionized (DI) water and dried in a vacuum oven. Then, the bottom Ni electrode was sealed with the CNT-coated fabric and VHB thin film.

Fabrication of Flexible Multipixel Arrays: The CNT-coated fabric was cut by a computer-controlled commercial CO₂ laser cutter system and then integrated in a 4×4 pixel arrays of interdigitated textile pixels and sandwiched between a VHB thin film, leading to large-area, patterned pressure sensors.

Characterization: The current intensity was measured by an electrochemical work station (CHI 760E) and a Keithley electrometer 6514. A LabVIEW controlled digital source meter (Keithley 2450) was used to measure the I - t curves in real-time. The SEM images were collected using a Hitachi SU8200. A step motor (Linmot E1100) was used to test the mechanical stability of the device.

Supporting Information

Supporting information is available from the Wiley Online Library or from the author.

Acknowledgements

The authors acknowledge the support from the “Thousands Talents” program for pioneer researcher and his innovation team, China, National Natural Science Foundation of China (Grant Nos. 51432005, 61574018, and 51603013), the Youth Innovation Promotion Association of CAS, “Hundred Talents Program” of CAS, and National Key Research and Development Program of China (No. 2016YFA0202703). Participants took part in the experiments described herein with informed consent. No formal approval for these experiments was required.

Conflict of Interest

The authors declare no conflict of interest.

Keywords

large-area, pressure sensors, smart textiles, wearable electronics

Received: July 3, 2017

Revised: August 4, 2017

Published online: September 26, 2017

- [1] C. S. Boland, U. Khan, G. Ryan, S. Barwich, R. Charifou, A. Harvey, C. Backes, Z. Li, M. S. Ferreira, M. E. Möbius, R. J. Young, J. N. Coleman, *Science* **2016**, 354, 1257.
- [2] a) D.-H. Kim, N. Lu, R. Ma, Y.-S. Kim, R.-H. Kim, S. Wang, J. Wu, S. M. Won, H. Tao, A. Islam, K. J. Yu, T.-i. Kim, R. Chowdhury, M. Ying, L. Xu, M. Li, H.-J. Chung, H. Keum, M. McCormick, P. Liu, Y.-W. Zhang, F. G. Omenetto, Y. Huang, T. Coleman, J. A. Rogers, *Science* **2011**, 333, 838; b) D. J. Lipomi, M. Vosgueritchian, B. C. Tee, S. L. Hellstrom, J. A. Lee, C. H. Fox, Z. Bao, *Nat. Nanotechnol.* **2011**, 6, 788; c) T. Yamada, Y. Hayamizu, Y. Yamamoto, Y. Yomogida, A. Izadi-Najafabadi, D. N. Futaba, K. Hata, *Nat. Nanotechnol.* **2011**, 6, 296.
- [3] M. Y. Lee, J. Hong, E. K. Lee, H. Yu, H. Kim, J. U. Lee, W. Lee, J. H. Oh, *Adv. Funct. Mater.* **2016**, 26, 1445.
- [4] a) X. Pu, M. Liu, L. Li, S. Han, X. Li, C. Jiang, C. Du, J. Luo, W. Hu, Z. L. Wang, *Adv. Energy Mater.* **2016**, 6, 1601254; b) X. Pu, L. Li, M. Liu, C. Jiang, C. Du, Z. Zhao, W. Hu, Z. L. Wang, *Adv. Mater.* **2016**, 28, 98; c) J. Chen, Y. Huang, N. Zhang, H. Zou, R. Liu, C. Tao, X. Fan, Z. L. Wang, *Nat. Energy* **2016**, 1, 16138; d) L. Liu, Y. Yu, C. Yan, K. Li, Z. Zheng, *Nat. Commun.* **2015**, 6, 7260; e) Q. Huang, D. Wang, Z. Zheng, *Adv. Energy Mater.* **2016**, 6, 1600783; f) X. Pu, W. Song, M. Liu, C. Sun, C. Du, C. Jiang, X. Huang, D. Zou, W. Hu, Z. L. Wang, *Adv. Energy Mater.* **2016**, 6, 1601048.
- [5] K. I. Jang, S. Y. Han, S. Xu, K. E. Mathewson, Y. Zhang, J. W. Jeong, G. T. Kim, R. C. Webb, J. W. Lee, T. J. Dawidczyk, R. H. Kim, Y. M. Song, W. H. Yeo, S. Kim, H. Cheng, S. I. Rhee, J. Chung, B. Kim, H. U. Chung, D. Lee, Y. Yang, M. Cho, J. G. Gaspar, R. Carbonari, M. Fabiani, G. Gratton, Y. Huang, J. A. Rogers, *Nat. Commun.* **2014**, 5, 4779.
- [6] a) S. Lee, A. Reuveny, J. Reeder, S. Lee, H. Jin, Q. Liu, T. Yokota, T. Sekitani, T. Isoyama, Y. Abe, Z. Suo, T. Someya, *Nat. Nanotechnol.* **2016**, 11, 472; b) A. Chortos, J. Liu, Z. Bao, *Nat. Mater.* **2016**, 15, 937.
- [7] a) G. Schwartz, B. C. Tee, J. Mei, A. L. Appleton, H. Kim do, H. Wang, Z. Bao, *Nat. Commun.* **2013**, 4, 1859; b) J. Lee, H. Kwon, J. Seo, S. Shin, J. H. Koo, C. Pang, S. Son, J. H. Kim, Y. H. Jang, D. E. Kim, T. Lee, *Adv. Mater.* **2015**, 27, 2433.
- [8] a) W. Wu, X. Wen, Z. L. Wang, *Science* **2013**, 340, 952; b) K.-Y. Shin, J. S. Lee, J. Jang, *Nano Energy* **2016**, 22, 95.
- [9] a) C. L. Choong, M. B. Shim, B. S. Lee, S. Jeon, D. S. Ko, T. H. Kang, J. Bae, S. H. Lee, K. E. Byun, J. Im, Y. J. Jeong, C. E. Park, J. J. Park, U. I. Chung, *Adv. Mater.* **2014**, 26, 3451; b) Y.-C. Lai, B.-W. Ye, C.-F. Lu, C.-T. Chen, M.-H. Jao, W.-F. Su, W.-Y. Hung, T.-Y. Lin, Y.-F. Chen, *Adv. Funct. Mater.* **2016**, 26, 1286.
- [10] a) X. Pu, M. Liu, X. Chen, J. Sun, C. Du, Y. Zhang, J. Zhai, W. Hu, Z. L. Wang, *Sci. Adv.* **2017**, 3, e1700015; b) S. W. Chen, X. Cao, N. Wang, L. Ma, H. R. Zhu, M. Willander, Y. Jie, Z. L. Wang, *Adv. Energy Mater.* **2017**, 7, 1601255; c) X. Wang, H. Zhang, L. Dong, X. Han, W. Du, J. Zhai, C. Pan, Z. L. Wang, *Adv. Mater.* **2016**, 28, 2896.
- [11] a) J. Kim, M. Lee, H. J. Shim, R. Ghaffari, H. R. Cho, D. Son, Y. H. Jung, M. Soh, C. Choi, S. Jung, K. Chu, D. Jeon, S. T. Lee, J. H. Kim, S. H. Choi, T. Hyeon, D. H. Kim, *Nat. Commun.* **2014**, 5, 5747; b) D.-Y. Khang, H. Jiang, Y. Huang, J. A. Rogers, *Science* **2006**, 311, 208.
- [12] S. C. Mannsfeld, B. C. Tee, R. M. Stoltenberg, C. V. Chen, S. Barman, B. V. Muir, A. N. Sokolov, C. Reese, Z. Bao, *Nat. Mater.* **2010**, 9, 859.
- [13] a) M. Kaltenbrunner, T. Sekitani, J. Reeder, T. Yokota, K. Kuribara, T. Tokuhara, M. Drack, R. Schwodiauer, I. Graz, S. Bauer-Gogonea, S. Bauer, T. Someya, *Nature* **2013**, 499, 458; b) E. Song, B. Kang, H. H. Choi, D. H. Sin, H. Lee, W. H. Lee, K. Cho, *Adv. Electron. Mater.* **2016**, 2, 1500250; c) B. Kang, F. Ge, L. Qiu, K. Cho, *Adv. Electron. Mater.* **2017**, 3, 1600240; d) I. Cho, S. K. Park, B. Kang, J. W. Chung, J. H. Kim, K. Cho, S. Y. Park, *Adv. Funct. Mater.* **2016**, 26, 2966.
- [14] J. Y. Sun, C. Keplinger, G. M. Whitesides, Z. Suo, *Adv. Mater.* **2014**, 26, 7608.
- [15] a) Y.-C. Lai, J. Deng, S. L. Zhang, S. Niu, H. Guo, Z. L. Wang, *Adv. Funct. Mater.* **2017**, 27, 1604462; b) M. Shi, J. Zhang, H. Chen, M. Han, S. A. Shankaregowda, Z. Su, B. Meng, X. Cheng, H. Zhang, *ACS Nano* **2016**, 10, 4083; c) W. Zeng, X.-M. Tao, S. Chen, S. Shang, H. L. W. Chan, S. H. Choy, *Energy Environ. Sci.* **2013**, 6, 2631.
- [16] a) D.-H. Kim, Y.-S. Kim, J. Wu, Z. Liu, J. Song, H.-S. Kim, Y. Y. Huang, K.-C. Hwang, J. A. Rogers, *Adv. Mater.* **2009**, 21, 3703; b) N. Luo, W. Dai, C. Li, Z. Zhou, L. Lu, C. C. Y. Poon, S.-C. Chen, Y. Zhang, N. Zhao, *Adv. Funct. Mater.* **2016**, 26, 1178; c) B. Zhu, Z. Niu, H. Wang, W. R. Leow, H. Wang, Y. Li, L. Zheng, J. Wei, F. Huo, X. Chen, *Small* **2014**, 10, 3625.
- [17] a) L. M. Castano, A. B. Flatau, *Smart Mater. Struct.* **2014**, 23, 053001; b) F. Wang, B. Zhu, L. Shu, X. Tao, *Smart Mater. Struct.* **2014**, 23, 015001; c) W. Zeng, L. Shu, Q. Li, S. Chen, F. Wang, X. M. Tao, *Adv. Mater.* **2014**, 26, 5310; d) W. Weng, P. Chen, S. He, X. Sun, H. Peng, *Angew. Chem., Int. Ed. Engl.* **2016**, 55, 6140.
- [18] a) S. Y. Kim, S. Park, H. W. Park, H. Park do, Y. Jeong, D. H. Kim, *Adv. Mater.* **2015**, 27, 4178; b) Z. Liu, D. Qi, P. Guo, Y. Liu, B. Zhu, H. Yang, Y. Liu, B. Li, C. Zhang, J. Yu, B. Liedberg, X. Chen, *Adv. Mater.* **2015**, 27, 6230.

- [19] a) F. Zhao, Y. Zhao, H. Cheng, L. Qu, *Angew. Chem., Int. Ed. Engl.* **2015**, 54, 14951; b) M. Nanjian, K. Xia, Q. Wang, Z. Yin, H. Wang, C. Wang, H. Xie, M. Zhang, Y. Zhang, *Adv. Funct. Mater.* **2017**, 27, 1606066; c) J. Mu, C. Hou, G. Wang, X. Wang, Q. Zhang, Y. Li, H. Wang, M. Zhu, *Adv. Mater.* **2016**, 28, 9491; d) C. Hou, H. Wang, Q. Zhang, Y. Li, M. Zhu, *Adv. Mater.* **2014**, 26, 5018.
- [20] a) Z. Lou, S. Chen, L. Wang, K. Jiang, G. Shen, *Nano Energy* **2016**, 23, 7; b) C. Yan, J. Wang, W. Kang, M. Cui, X. Wang, C. Y. Foo, K. J. Chee, P. S. Lee, *Adv. Mater.* **2014**, 26, 2022.
- [21] C. Wang, X. Li, E. Gao, M. Jian, K. Xia, Q. Wang, Z. Xu, T. Ren, Y. Zhang, *Adv. Mater.* **2016**, 28, 6640.
- [22] C. Pang, G. Y. Lee, T. I. Kim, S. M. Kim, H. N. Kim, S. H. Ahn, K. Y. Suh, *Nat. Mater.* **2012**, 11, 795.
- [23] J. Ge, L. Sun, F. R. Zhang, Y. Zhang, L. A. Shi, H. Y. Zhao, H. W. Zhu, H. L. Jiang, S. H. Yu, *Adv. Mater.* **2016**, 28, 722.
- [24] a) M. M. Hamed, A. Ainla, F. Guder, D. C. Christodouleas, M. T. Fernandez-Abedul, G. M. Whitesides, *Adv. Mater.* **2016**, 28, 5054; b) L. Pan, A. Chortos, G. Yu, Y. Wang, S. Isaacson, R. Allen, Y. Shi, R. Dauskardt, Z. Bao, *Nat. Commun.* **2014**, 5, 3002.
- [25] C. Wang, M. Zhang, K. Xia, X. Gong, H. Wang, Z. Yin, B. Guan, Y. Zhang, *ACS Appl. Mater. Interfaces* **2017**, 9, 13331.
- [26] S. Gong, W. Schwalb, Y. Wang, Y. Chen, Y. Tang, J. Si, B. Shirinzadeh, W. Cheng, *Nat. Commun.* **2014**, 5, 3132.
- [27] G. Y. Bae, S. W. Pak, D. Kim, G. Lee, D. H. Kim, Y. Chung, K. Cho, *Adv. Mater.* **2016**, 28, 5300.
- [28] a) K. Takei, T. Takahashi, J. C. Ho, H. Ko, A. G. Gillies, P. W. Leu, R. S. Fearing, A. Javey, *Nat. Mater.* **2010**, 9, 821; b) Q. Cao, S. H. Hur, Z. T. Zhu, Y. G. Sun, C. J. Wang, M. A. Meitl, M. Shim, J. A. Rogers, *Adv. Mater.* **2006**, 18, 304.
- [29] X. Wang, Y. Gu, Z. Xiong, Z. Cui, T. Zhang, *Adv. Mater.* **2014**, 26, 1336.
- [30] C. Wang, D. Hwang, Z. Yu, K. Takei, J. Park, T. Chen, B. Ma, A. Javey, *Nat. Mater.* **2013**, 12, 899.
- [31] D. Kang, P. V. Pikhitsa, Y. W. Choi, C. Lee, S. S. Shin, L. Piao, B. Park, K. Y. Suh, T. I. Kim, M. Choi, *Nature* **2014**, 516, 222.
- [32] X. Pu, L. Li, H. Song, C. Du, Z. Zhao, C. Jiang, G. Cao, W. Hu, Z. L. Wang, *Adv. Mater.* **2015**, 27, 2472.
- [33] L. Hu, M. Pasta, F. L. Mantia, L. Cui, S. Jeong, H. D. Deshazer, J. W. Choi, S. M. Han, Y. Cui, *Nano Lett.* **2010**, 10, 708.